J|A|C|S
ARTICLES
Published on Web 12/04/2001

Role of Framework Sodium versus Local Framework Structure in Determining the Hydrothermal Stability of MCM-41 Mesostructures

Thomas R. Pauly,[†] Valeri Petkov,[‡] Yu Liu,[†] Simon J. L. Billinge,*[,‡] and Thomas J. Pinnavaia*[,†]

Contribution from the Department of Chemistry, Department of Physics and Astronomy, and Center for Fundamental Materials Research, Michigan State University, East Lansing, Michigan 48824

Received July 26, 2001

Abstract: Two mesostructured MCM-41 silicas that differ dramatically in hydrothermal stability have been examined by ^{29}Si MAS NMR spectroscopy and pair distribution function (PDF) analysis of synchrotron X-ray scattering data. The less stable mesostructure assembled from sodium silicate and the substantially more stable derivative made from fumed silica possess equivalent local framework wall structures, as judged by NMR and PDF methods. Approximately 80% of the SiO_4 tetrahedra are fully cross-linked as Q^4 ($Si(OSi)_4$) units in both calcined samples. Additionally, the structural correlation distances for the two materials are nearly identical, having values of 1.62(1), ~2.60, and 3.09(1) Å for the Si−O, O−O, and nearest neighbor Si−Si distances in the framework. Sodium ions in the framework play a crucial role in limiting the hydrothermal stability of the mesostructure. Residual sodium (~0.05−0.10% Na_2O) is retained in the MCM-41 made from sodium silicate, even after two ion exchange reactions with ammonium ions in more than 300 − fold excess. The entrapped framework sodium ions catalyze the collapse of the mesopores upon exposure to 20% steam at 800 °C for 5 h. The sodium − free mesostructure assembled from fumed silica retains an open framework under the same hydrothermal conditions. The stability of the fumed silica derivative, however, is greatly compromised when doped with as little as 0.10% Na_2O, thus confirming the deleterious effect of sodium on hydrothermal stability.

Introduction

The assembly of MCM-41 and related mesostructured silicas[1,2] normally is accomplished through a cooperative supramolecular assembly mechanism that incorporates electrostatic interactions between the charged headgroups of lyotropic organic micelles and silicate precursors in solution.[3−5] Nonionic assembly pathways also have been developed wherein hydrogen bonding[6,7] and dative bonding[8,9] interactions are used to unite silica precursors with surfactant headgroups at the micelle−solution interface. Substantial differences in both framework access and thermal/hydrothermal stability have been observed for mesostructured silicas assembled through electrostatic and hydrogen bonding pathways. The differences in framework access, which are reflected in part by differences in catalytic activity,[10−12] can be explained on the basis of differences in the pore network, pore diameter, and, most importantly, pore length. However, the differences in thermal and hydrothermal stability for silica mesostructures assembled through ionic and nonionic assembly mechanisms is less well understood.

At least four factors are expected to influence the stability of a mesostructured silica framework, namely, (i) the degree of overall framework cross-linking, (ii) the local structure and connectivity of the silicate subunits comprising the framework walls, (iii) the framework wall thickness, and (iv) the nature of the countercations balancing the charge on the framework walls. The importance of framework cross-linking is reflected in the fact that nonionic assembly pathways typically afford more stable mesostructures in comparison to electrostatically assembled analogues, because the need for ionic charge matching

[†] Department of Chemistry.
[‡] Department of Physics and Astronomy and Center for Fundamental Materials Research.

(1) Beck, J. S.; Vartuli, J. C.; Roth, W. J.; Leonowicz, M. E.; Kresge, C. T.; Schmitt, K. D.; Chu, C. T. W.; Olson, D. H.; Sheppard, E. W.; et al. *J. Am. Chem. Soc.* **1992**, *114*, 10834−10843.
(2) Inagaki, S.; Fukushima, Y.; Kuroda, K. *Stud. Surf. Sci. Catal.* **1994**, *84*, 125−132.
(3) Monnier, A.; Schuth, F.; Huo, Q.; Kumar, D.; Margolese, D.; Maxwell, R. S.; Stucky, G. D.; Krishnamurty, M.; Petroff, P.; et al. *Science (Washington, D.C., 1883−)* **1993**, *261*, 1299−1303.
(4) Chen, C. Y.; Burkett, S. L.; Li, H. X.; Davis, M. E. *Microporous Mater.* **1993**, *2*, 27−34.
(5) Huo, Q.; Margolese, D. I.; Ciesla, U.; Feng, P.; Gier, T. E.; Sieger, P.; Leon, R.; Petroff, P. M.; Schueth, F.; Stucky, G. D. *Nature (London)* **1994**, *368*, 317−321.
(6) Tanev, P. T.; Pinnavaia, T. J. *Science (Washington, D.C.)* **1995**, *267*, 865−867.
(7) Bagshaw, S. A.; Prouzet, E.; Pinnavaia, T. J. *Science (Washington, D.C.)* **1995**, *269*, 1242−1244.
(8) Antonelli, D. M.; Nakahira, A.; Ying, J. Y. *Inorg. Chem.* **1996**, *35*, 3126−3136.
(9) Antonelli, D. M.; Ying, J. Y. *Chem. Mater.* **1996**, *8*, 874−881.
(10) Pinnavaia, T. J.; Zhang, W. *Stud. Surf. Sci. Catal.* **1998**, *117*, 23−36.
(11) Yang, R. T.; Pinnavaia, T. J.; Li, W.; Zhang, W. *J. Catal.* **1997**, *172*, 488−493.
(12) Pauly, T. R.; Liu, Y.; Pinnavaia, T. J.; Billinge, S. J. L.; Rieker, T. P. *J. Am. Chem. Soc.* **1999**, *121*, 8835−8842.

of incompletely cross-linked Q^3 units is eliminated.[13,14] Recently reports[15−18] of the use of protozeolitic silicate seeds for the assembly of steam stable mesostructures clearly point to the importance of the silicate subunit connectivity. Also, it is clear that structures with thicker walls will take longer to degrade in comparison to thin-walled analogues,[13,19,20] though the microscopic rate constants for degradation will be independent of wall thickness.

Several studies[21−29] have pointed to the importance of the countercations balancing the silicate charge on the framework walls. For instance, MCM-41 silicas assembled from sodium silicate are typically less stable than structurally equivalent analogues prepared from fumed silica in the absence of sodium. This implies that the small amount of sodium that inevitably is incorporated into the framework of a mesostructure assembled from sodium silicate may catalyze the collapse of the framework under hydrothermal conditions. Alternatively, the framework subunits derived from fumed silica may have local structures that are fundamentally different and intrinsically more stable in comparison to mesostructures derived from sodium silicate. Distinguishing between these two later possibilities would provide useful insights into the factors that contribute to the relative hydrothermal stabilities of mesostructured silicates.

In the present work we use NMR spectroscopy, pair distribution function (PDF) analysis of synchrotron X-ray powder diffraction, and other physical methods to examine the local structures of MCM-41 silica mesostructures assembled from fumed silica and sodium silicate precursors. We also have investigated the effect of sodium silicate doping on hydrothermal stability. The results indicate that the difference in hydrothermal stability between MCM-41 mesostructures assembled from fumed silica and sodium silicate are determined primarily by the presence or absence of sodium in the framework and less so on the local subunit structures provided by these two silica precursors.

Experimental Section

MCM-41 Assembled from Sodium Silicate. A 37.1-g quantity of sodium silicate (27% SiO_2, 14% NaOH, Aldrich) was added to 200 mL of H_2O and stirred for 15 min. A second solution of 15.9 g of cetyltrimethylammonium bromide (CTAB) in 100 mL of H_2O was prepared by warming the mixture to 45 °C to dissolve the template. The surfactant solution then was added to the silicate solution and stirred for 30 min. The pH of the mixture was adjusted to a value of 11 through the dropwise addition of 4.06 g of H_2SO_4 (98%) in 30 mL of H_2O over a 30-min period. The reaction vessel was sealed and heated to 100 °C. After 24 h, the reaction vessel was allowed to cool to 65 °C and the pH was again adjusted to 10 with the addition of 1.00 g of H_2SO_4 (98%) in 20 mL of H_2O. This process of adjusting the pH in an incremental fashion has been used previously to obtain high-quality MCM-41.[30] The reaction vessel was again sealed and the mixture was heated at 100 °C for an additional 24 h. The final stoichiometry of the reaction mixture was 1.00 SiO_2:0.39 Na_2O:0.26 CTAB:0.30 H_2SO_4: 66.0 H_2O. The solid products were recovered by filtration, washed with copious amounts of distilled H_2O, air-dried at 25 °C for 24 h, and calcined at 600 °C for 4 h in air to remove the surfactant and cross-link the framework.

MCM-41 Assembled from Fumed Silica. A MCM-41 sample was prepared from fumed silica by using the procedure outlined by Klinowski et al.[27] A solution containing 11.7 g of TMAOH (25% in H_2O) and 16.40 g of CTABr was added to 125 mL of deionized H_2O with stirring at 45 °C until the surfactant dissolved. To this solution was added 10.0 g of fumed silica (99.8%, Aldrich) to bring the reaction stoichiometry to the following molar ratios: 1.00 SiO_2: 0.19 TMAOH: 0.28 CTAB: 53 H_2O. The mixture was stirred for 2 h, aged statically at 20 °C for 24 h, and then heated statically in a Teflon-lined stainless steel autoclave at 150 °C under autogenous pressure for 48 h. The solid product was recovered by filtration, washed with copious amounts of H_2O, air-dried at 25 °C for 24 h, and calcined at 600 °C for 4 h in air to remove the surfactant and cross-link the framework.

NH_4^+ Exchange for Na^+. A 0.50-g quantity of calcined MCM-41 prepared from sodium silicate was added to 20 mL of 0.50 M NH_4Cl solution and the mixture was stirred for 2 h. The solid was recovered by filtration and washed with copious amounts of H_2O. The exchange reaction was repeated a second time. The solid was air-dried for 24 h and then calcined at 500 °C for 4 h to convert the ammonium exchange cations to protons. EDS analysis indicated that the Na_2O content in the mesostructure decreased from an initial value of about 0.25 mol % to about 0.05−0.1 mol % as a result of the ion exchange process.

Sodium Silicate Doping. A 0.20-g quantity of calcined MCM-41 prepared from fumed silica was added to 1.0 mL of aqueous solutions of 3.2×10^{-3} M and 1.6×10^{-2} M Na_2O from Na_2SiO_3 (Aldrich) and stirred at ambient temperature overnight. The suspensions were allowed to evaporate and the dried samples were calcined at 500 °C for 4 h, affording derivatives doped with 0.10 and 0.50 mol % Na_2O.

Steaming Experiments. The MCM-41 samples where subjected to 20% H_2O vapor in a N_2 stream at 800 °C for 5 h. The nitrogen stream was bubbled through a water bath at a controlled temperature to achieve the desired partial pressure of water vapor.

Physical Measurements. In-house X-rays were used for basic characterization of the sample. The wide-angle powder X-ray diffraction (XRD) patterns were obtained with a Rigaku Rotaflex Diffractometer with Cu Kα radiation ($\lambda = 0.154$ nm). Counts were accumulated every 0.02° (2θ) at a scan speed of 1° (2θ)/min.

N_2 adsorption−desorption isotherms were obtained at −196 °C on a Micromeritics ASAP 2010 Sorptometer following static adsorption procedures. Samples were outgassed at 150 °C and 10^{-6} Torr for a minimum of 12 h prior to analysis. BET surface areas were calculated from the linear part of the BET plot according to IUPAC[31] recommendations. Pore size distribution was estimated from the adsorption branch of the isotherm by the method of Horvath and Kawazoe.[32]

(13) Tanev, P. T.; Pinnavaia, T. J. *Chem. Mater.* **1996**, *8*, 2068−2079.
(14) Kim, S. S.; Zhang, W.; Pinnavaia, T. J. *Science (Washington, D.C.)* **1998**, *282*, 1302−1305.
(15) Liu, Y.; Zhang, W.; Pinnavaia, T. J. *Angew. Chem., Int. Ed.* **2001**, *40*, 1255−1258.
(16) Liu, Y.; Zhang, W.; Pinnavaia, T. J. *J. Am. Chem. Soc.* **2000**, *122*, 8791−8792.
(17) Zhang, Z.; Han, Y.; Xiao, F.-S.; Qiu, S.; Zhu, L.; Wang, R.; Yu, Y.; Zhang, Z.; Zou, B.; Wang, Y.; Sun, H.; Zhao, D.; Wei, Y. *J. Am. Chem. Soc.* **2001**, *123*, 5014−5021.
(18) Zhang, Z.; Han, Y.; Zhu, L.; Wang, R.; Yu, Y.; Qiu, S.; Zhao, D.; Xiao, F.-S. *Angew. Chem., Int. Ed.* **2001**, *40*, 1258−1262.
(19) Cheng, C.-F.; Zhou, W.; Park, D. H.; Klinowski, J.; Hargreaves, M.; Gladden, L. F. *J. Chem. Soc., Faraday Trans.* **1997**, *93*, 359−363.
(20) He, N.; Lu, Z.; Yuan, C.; Hong, J.; Yang, C.; Bao, S.; Xu, Q. *Supramol. Sci.* **1998**, *5*, 553−558.
(21) Kim, J. M.; Kwak, J. H.; Jun, S.; Ryoo, R. *J. Phys. Chem.* **1995**, *99*, 16742−16747.
(22) Ryoo, R.; Kim, J. M.; Ko, C. H. *Stud. Surf. Sci. Catal.* **1998**, *117*, 151−158.
(23) Kruk, M.; Jaroniec, M.; Ryoo, R.; Kim, J. M. *Microporous Mater.* **1997**, *12*, 93−106.
(24) Corma, A.; Kan, Q.; Navarro, M. T.; Perez-Pariente, J.; Rey, F. *Chem. Mater.* **1997**, *9*, 2123-2126.
(25) Ryoo, R.; Jun, S. *J. Phys. Chem. B* **1997**, *101*, 317−320.
(26) Kim, J. M.; Jun, S.; Ryoo, R. *J. Phys. Chem. B* **1999**, *103*, 6200−6205.
(27) Cheng, C.-F.; Park Dong, H.; Klinowski, J. *J. Chem. Soc., Faraday Trans.* **1997**, *93*, 193−197.
(28) Lin, W.; Cai, Q.; Pang, W.; Yue, Y.; Zou, B. *Microporous Mesoporous Mater.* **1999**, *33*, 187−196.
(29) Chen, L.; Horiuchi, T.; Mori, T.; Maeda, K. *J. Phys. Chem. B* **1999**, *103*, 1216−1222.
(30) Ryoo, R.; Kim, J. M. *J. Chem. Soc., Chem. Commun.* **1995**, 711−712.
(31) Sing, K. S. W.; Everett, D. H.; Haul, R. A. W.; Moscou, L.; Pierotti, R. A.; Rouquerol, J.; Siemieniewska, T. *Pure Appl. Chem.* **1985**, *57*, 603−619.
(32) Horvath, G.; Kawazoe, K. *J. Chem. Eng. Jpn.* **1983**, *16*, 470−475.

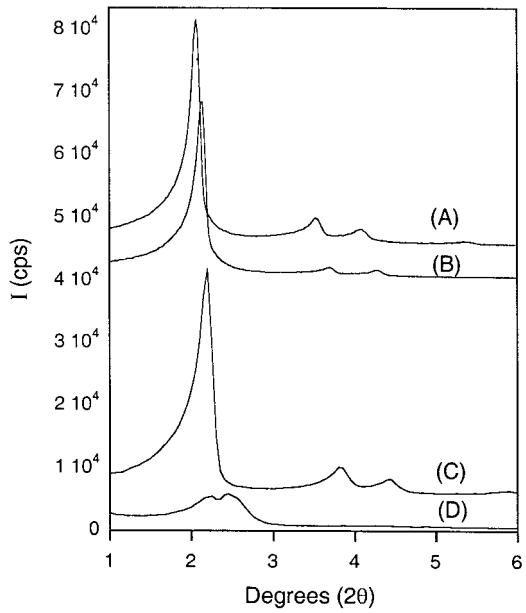

Figure 1. Wide-angle powder X-ray diffraction patterns for calcined MCM-41 assembled from fumed silica (A) before exposure to 20% steam and (B) after exposure to 20% steam at 800 °C for 5 h. Patterns C and D are for calcined MCM-41 assembled from sodium silicate under the corresponding conditions.

^{29}Si MAS NMR spectra were recorded on a Varian 400 VRX solid-state NMR Spectrometer at 79.5 MHz under single-pulse mode with a 7-mm Zirconia rotor, a spinning frequency of 4 kHz, pulse width of 8.5 μs, and a pulse delay of 870 s. The chemical shifts where externally referenced to talc (−98.1 ppm relative to tetramethylsilane).

Semiquantitative analyses for sodium were performed with use of a JEOL JSM-35C scanning electron microscope (SEM) equipped with a Tracor Northern energy dispersive spectroscopy (EDS) detector. Data acquisition was performed no less than 6 times in different areas of the samples with an accelerating voltage of 20 kV and a 60 s accumulation time.

Accurate high-resolution PDF measurements require data with good statistics to be measured over a wide range of momentum transfer, Q.[33] Weakly scattering samples, such as these low-density mesostructured silicas of interest in the present work, require the use of synchrotron sources. The data for these measurements were obtained at the MuCAT undulator beam line ID6 at the Advanced Photon Source, Argonne National Laboratories. The measurements were obtained by using symmetric transmission geometry and X-rays of energy 40 keV. Although the samples were very low density and silica is weakly scattering, the very high flux of high-energy X-rays from this beamline allowed structure data with adequate statistics to be obtained to a Q_{max} of 22 A^{-1}. Diffracted X-ray photons were collected with a scintillation counter connected to a single channel analyzer. Several diffraction runs were conducted and the diffraction spectra averaged to improve the statistical accuracy and reduce any systematic effect due to instabilities in the experimental setup. The data were normalized for flux, corrected for detector dead time, for background and Compton scattering, and for absorption, and then converted to total scattering structure factors, $S(Q)$,[34]

$$S(Q) = 1 + [I^{el.}(Q) - \sum c_i|f_i(Q)|^2]/|\sum c_i f_i(Q)|^2 \qquad (1)$$

where c_i and f_i are the atomic concentration and scattering factor, respectively, for the atomic species of type i (i = Si, O), $I^{el.}(Q)$ is the total diffracted intensity, and Q is the magnitude of the wave vector.

(33) Egami, T., Ed. *Local Structure From Diffraction*; Plenum: New York, 1998.
(34) Warren, B. E. *X-ray Diffraction*; Dover: New York, 1990.

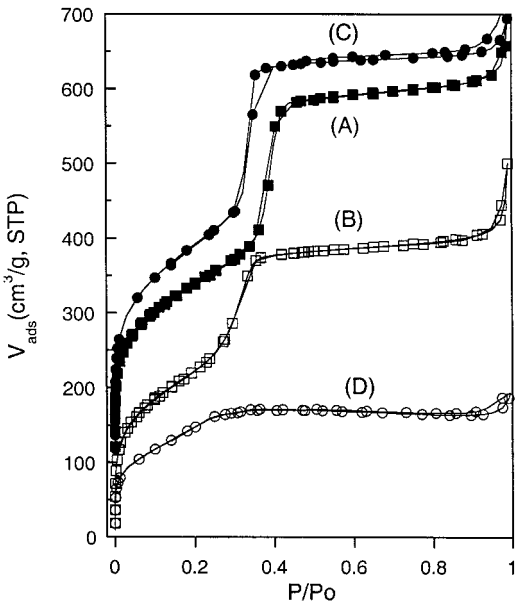

Figure 2. N_2 adsorption−desorption isotherms of calcined MCM-41 assembled from fumed silica (A) before and (B) after exposure to 20% steam at 800 °C for 5 h. Isotherms C and D are the corresponding isotherms for MCM-41assembled from sodium silicate. The isotherms for MCM-41 assembled from fumed silica are offset by 100 cm^3/g.

The PDFs, $G(r)$, were obtained from the sine Fourier transform of $S(Q)$ according to

$$G(r) = (2/\pi) \int_{Q_{max}}^{Q=0} Q[S(Q) - 1]\sin(Qr)\, dQ \qquad (2)$$

The PDF has peaks at characteristic distances separating pairs of atoms. Thus, the position of a peak in the PDF gives the most frequently occurring interatomic distances and the area under the peak provides the number of atomic neighbors for that distance.

All data processing was done with the help of the program RAD.[35]

Results

To investigate the amorphous wall structures of MCM-41 silicas with significantly different hydrothermal stabilities, two mesostructured samples were assembled by using fumed silica and sodium silicate as the silica precursors. Figure 1 shows the wide-angle powder X-ray diffraction patterns for each sample after calcination at 600 °C and after exposure to 20% steam at 800 °C for 5 h. Both calcined samples exhibited good long-range hexagonal order as evidenced by the presence of four Bragg reflections. After steaming, however, the MCM-41 derived from sodium silicate showed a significant decrease in intensity of the *100* peak and the disappearance of all higher order reflections. In comparison, the sample assembled from fumed silica retained three reflections after steaming and showed only small changes in the position and intensity of the *100* refection.

The N_2 adsorption−desorption isotherms shown in Figure 2 confirm the difference in hydrothermal stability for the two forms of MCM-41. Both samples in calcined form exhibited Type IV isotherms with capillary condensation steps occurring at a partial pressure corresponding to Horvath−Kawazoe pore size distributions centered between 3.5 and 4.0 nm. Both samples showed only a small uptake of N_2 at higher partial pressures,

(35) Petkov, V. *J. Appl. Crystallogr.* **1989**, *22*, 387−389.

Table 1. Physiochemical Properties of Calcined and Steamed Samples of MCM-41 Assembled from Sodium Silicate and Fumed Silica as Silica Precursors

silica precursor	pore vol (mL/g)[c]	pore size (nm)[d]	a_o (nm)[e]	wall thickness (nm)[f]	BET SA (m_2/g)	NMR Q^4/Q^3	mol % Na_2O
sodium silicate							
calcined sample[a]	0.83	3.6	4.7	1.1	1052	4.1	0.20(5)
steamed sample[b]	0.26 (31%)[g]	2.2	N/A	N/A	550 (52%)[g]	N/A	N/A
fumed silica							
calcined sample[a]	0.75	4.0	5.0	1.0	860	4	0.00(0)
steamed sample[b]	0.59 (79%)[g]	3.3	4.8	1.5	828 (96%)[g]	N/A	N/A

[a] Sample calcined at 600 °C in air for 6 h. [b] Calcined sample exposed to 20% H_2O vapor in a N_2 stream at 800 °C for 5 h. [c] Framework pore volume taken as the volume adsorbed at $P/P_o = 0.50$. [d] Pore size distribution determined by the Horvath and Kawazoe method.[31] [e] Lattice parameter of hexagonal cell, $a_o = d_{100} \cdot (3/2)^{1/2}$. [f] Wall thickness = a_o − pore diameter. [g] The values in parentheses represent the fraction of the surface area and pore volume retained after exposure to steam.

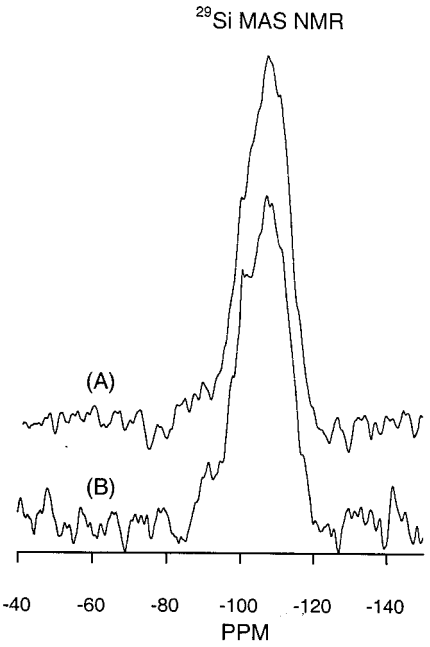

Figure 3. ^{29}Si MAS NMR spectra for calcined MCM-41 mesostructures assembled from (A) sodium silicate and (B) fumed silica. The Q^4 and Q^3 Si-resonances appear at −108 and −99.0 ppm, respectively.

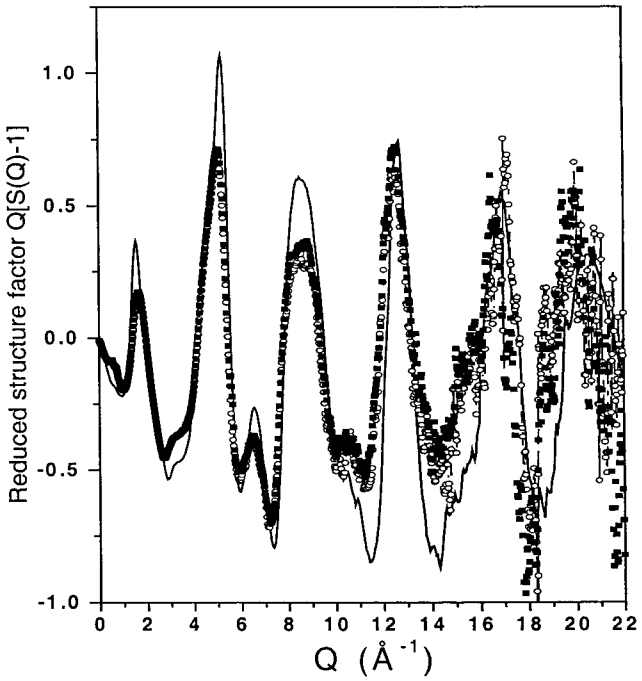

Figure 4. Experimental reduced structure factors for bulk silica (solid line), MCM-41 assembled from sodium silicate (open symbols), and MCM-41assembled from fumed silica (closed symbols).

consistent with the presence of relatively large monolithic particles (>300−500 nm) and the absence of interparticle textural porosity. The isotherms of the steamed samples, however, showed that the framework pores of the MCM-41 assembled from sodium silicate have almost completely collapsed, whereas the sample prepared from fumed silica retained most of its porosity. Table 1 compares the pore volumes, pore sizes, BET surface areas, and other physical properties of the two mesostructures before and after exposure to 20% steam at 800 °C.

Figure 3 provides the ^{29}Si MAS NMR spectra of the calcined MCM-41 materials. The spectra are nearly identical with regard to the chemical shift position and breadth of the resonance band. As expected based on the similarities in the NMR spectra, deconvolution of the spectra yields Q^4/Q^3 values of 4.1 and 4.0 for MCM-41 made from sodium silicate and fumed silica, respectively. This suggests that the cross-linking of the framework walls, as reflected in the distribution of incompletely cross-linked Q^3 and completely cross-linked Q^4 sites, is essentially independent of the silica source used in the assembly process once the cross-linking has been optimized through calcination.

To obtain information on the local structure of the framework walls for the two MCM-41 derivatives, we obtained the pair distribution functions for the mesostructures and compared the results with those that we previously reported for a bulk silica glass.[36] As can be seen in Figure 4, the experimental structure factors for the mesostructures mimic bulk silica glass by exhibiting prominent oscillations up to the maximum accessible Q value. Such oscillations result from the presence of well-defined subunits (namely, linked SiO_4 tetrahedra) comprising the framework walls. The peaks for the bulk silica glass below 10 A^{-1} are slightly sharper than the mesoporous silicas, indicating a greater degree of intermediate range order in the bulk glass in comparison to the mesostructures. Also, the wavelengths of the oscillations are slightly different between the bulk and mesoporous silicas. The scattering intensity for the mesoporous silicas is significantly lower than that for the bulk glass, especially at high Q. This reflects the difficulty of measuring samples with high void volume (low density) and thus low scattering power. Despite being clearly distinguishable from bulk silica glass, the mesostructures assembled from sodium silicate and fumed silica exhibit very similar structure functions, including the amplitude and frequency of the oscillations.

(36) Petkov, V.; Billinge, S. J. L.; Shastri, S. D.; Himmel, B. *Phys. Rev. Lett.* **2000**, *85*, 3436−3439.

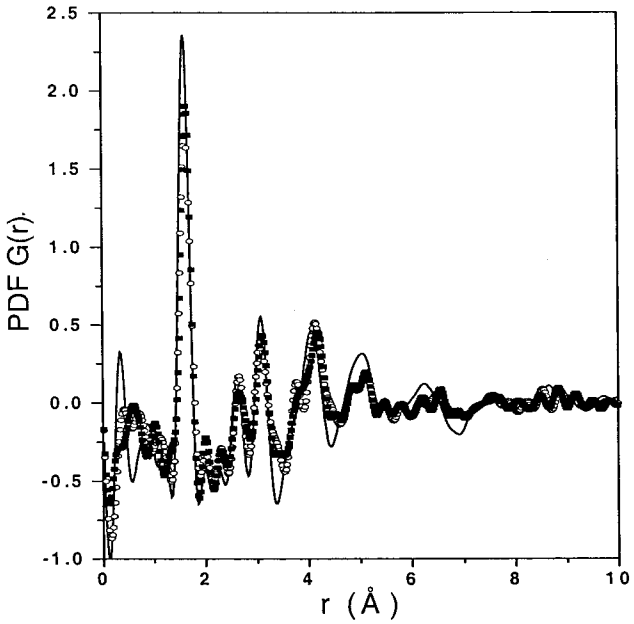

Figure 5. Experimental atomic PDF, *G*(r), for bulk silica (solid line), MCM-41 assembled from sodium silicate (open symbols), and MCM-41assembled from fumed silica (closed symbols).

The PDF profiles obtained from these structure functions are shown in Figure 5. The similarities in the PDF data verify that all three materials are made up of a random network of SiO_4 tetrahedral units.[36] Again, there are clear distinctions between the bulk and mesostructured silicas, but the two mesoporous silicas have virtually identical PDF profiles. The sharp peak near 1.6 Å comes from the well-defined Si−O bond in the materials. Peaks near 2.6 and 3.1 Å originate from O−O pairs on the tetrahedra and nearest neighbor Si−Si pairs, respectively. Peaks at higher *r* values also have structural significance (e.g., silicon to oxygen on neighboring tetrahedra between 4 and 5 Å); however, all structural peaks have died out by 8−10 Å in the bulk silica and by ∼6 Å in the mesoporous silicas. The shorter structural coherence in the mesostructured silicas reflects the less sharp features in *S*(*Q*) originating from a broader distribution of Si−O−Si bond angles resulting in less well-defined distances between second-neighbor tetrahedra. Indeed, this is borne out by a broader Si−Si peak at 3.1 Å for the mesoporous silicas.

We next investigated the sodium content of the two MCM-41 samples by EDS methods. No sodium was detected in the MCM-41 prepared from fumed silica, as would be expected in an alkali metal-free synthesis. However, sodium was present in the MCM-41 sample prepared from sodium silicate (Table 1). Attempts to remove all of the sodium ions by exchange with NH_4Cl failed. Analysis of the sample after two ion exchange reactions with 0.50 M NH_4Cl resulted in a reduction in the sodium content from an initial value of ∼0.25 mol % to ∼0.05−0.10 mol % Na_2O. This result indicated that a substantial fraction of the sodium is embedded in the framework walls.

Additional insights into the effect of sodium on the hydrothermal stability of MCM-41 were provided by doping a "stable" MCM-41 silica prepared from fumed silica with 0.50 and 0.1 mol % Na_2O to mimic the composition of MCM-41 assembled from sodium silicate before and after ion exchange with NH_4Cl. Figures 6 and 7 present the XRD and nitrogen isotherms for the pristine and doped versions of the mesostructure. Clearly,

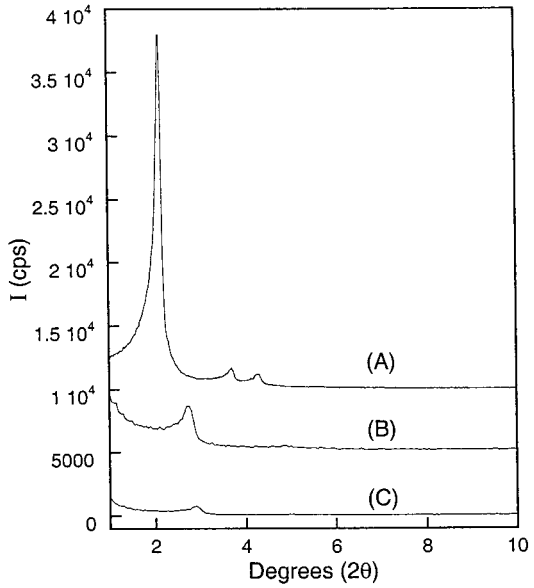

Figure 6. Wide-angle powder X-ray diffraction patterns for calcined MCM-41 assembled from fumed silica and exposed to 20% steam at 800 °C for 5 h: (A) sodium (Na^+) free, (B) doped with 0.1% Na_2O, (C) doped with 0.5% Na_2O (patterns are offset 5000 counts for clarity).

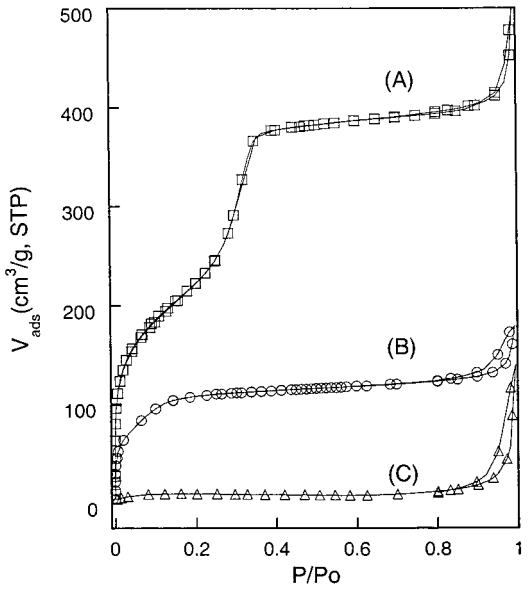

Figure 7. N_2 adsorption−desorption isotherms of calcined MCM-41 assembled from fumed silica and exposed to 20% steam at 800 °C for 5 h: (A) sodium (Na^+) free, (B) doped with 0.1% Na_2O, and (C) doped with 0.5% Na_2O.

the addition of as little as 0.1 mol % Na_2O greatly reduces the hydrothermal stability of the "stable" mesostructure.

Discussion

The assembly of MCM-41 from sodium silicate and fumed silica involved not only the use of different silica precursors, but also the use of different conditions of concentration, temperature, and pH. It is not surprising, therefore, that the calcined forms of the mesostructured products differed in terms of their textural properties as set out in Table 1. However, the difference in the hydrothermal stability of these two derivatives is far more dramatic and far beyond the differences observed in the textural properties. The calcined MCM-41 assembled from

fumed silica retains a hexagonal structure as well as 80% of its framework pore volume and more than 95% of its surface area after exposure to 20% steam in nitrogen at 800 °C for 5 h. In contrast, the mesostructured properties of the MCM-41 assembled from sodium silicate are greatly compromised after steaming under equivalent conditions, even though this derivative in calcined form exhibits an initially higher surface area and pore volume (cf., Table 1, Figures 1 and 2).

Differences in the framework wall thickness or the degree of framework cross-linking are precluded as possible reasons for the dramatic difference in hydrothermal stability. The wall thickness differs by no more than 10% for the two derivatives, 1.1 nm for the less stable derivative made from sodium silicate versus 1.0 nm for the more stable material built from fumed silica. About 80% of the SiO_4 tetrahedra in both materials are fully cross-linked as Q^4 $Si(OSiO_3)_4$ sites, as judged through the deconvolution of the ^{29}Si NMR spectra (cf., Figure 3, Table 1).

The experimental structure factors and PDF profiles shown in Figures 4 and 5, respectively, indicate that the two MCM-41 derivatives bear a structural resemblance to bulk silica glass insofar as all three materials are composed of a network of SiO_4 tetrahedra. However, the open framework mesostructures are easily distinguished from the dense glass on the basis of the PDF profiles. All of the PDF peaks for the mesostructured silicas are shifted to slightly higher *r* values relative to the bulk glass. This is especially apparent in the nearest-neighbor Si−O peak. The length of the Si−O bond in pure bulk silica glass is 1.60(1) Å from our data,[36] and in good agreement with literature values.[37] A fit to the Si−O peak in the mesostructures indicates an average bond length of 1.62(1) and 1.63(1) Å for the MCM-41 derived from sodium silicate and fumed silicas, respectively, which is slightly longer than that for the bulk glass. We believe that this bond lengthening is significant, because differences in the wavelengths of the oscillations in *S*(*Q*) are clearly visible for the bulk and mesostructured silicas (cf., Figure 4). It has been predicted theoretically that as the void space within a silica matrix increases, the Si−O bond length will increase.[38]

The PDF results also show that the mean Si−Si distance is longer for MCM-41 assembled from sodium silicate and fumed silica (3.08(1) and 3.10(1) Å, respectively) compared to the bulk silica (3.06(1) Å). In addition, the distribution of the Si−Si distance is broader in the mesostructures compared to the bulk glass. Because the integrated intensity under a PDF peak gives a quantitative measure of the multiplicity of that pair of atoms, we are able to estimate the coordination number for the pair.[33] By integrating the first peak in the PDF's we find that the average number of Si atoms around each oxygen in the bulk silica sample is 2.00(2), indicating a fully connected Q^4 network with each oxygen bridging two SiO_4 tetrahedra. On the other hand, in the MCM-41 derivatives made from sodium silicate and fumed silica the oxygen coordination number is 1.80(2) and 1.79(2), respectively. The lower coordination of oxygen is consistent with around 20% of the oxygen atoms being nonbridging atoms in incompletely cross-linked Q^3 tetrahedra of the type $OSi(OSiO_3)_3$. This PDF result is in agreement with the degree of framework cross-linking determined by NMR.

The Si−O bond lengths, the coordination numbers of the framework oxygen atoms, and the Si−O−Si bond angles as reflected in the Si−Si distances all indicate that the mesoporous silicas are more disordered and less perfect network structures than the bulk glass. Similar general findings have been recently reported on the basis of correlation function analysis of the XRD scattering properties of MCM-41 in comparison to bulk glass.[39] In view of the similarities in these structural parameters, and despite the dramatic difference in hydrothermal stability, the MCM-41 mesostructures derived from sodium silicate and fumed silica are essentially indistinguishable. Consequently, the observed difference in hydrothermal stability cannot be ascribed to a gross difference in the local atomic structure of the pore walls.

The comparatively poor hydrothermal stability of MCM-41 assembled from sodium silicate most likely arises from the retention of sodium ions in the framework walls of the resulting mesostructure. As estimated on the basis of EDS analysis, the mesostructure prepared from sodium silicate under the conditions used in this study contained about 0.25 mol % Na_2O, even though the as made material was washed with copious amounts of water. At least 20% of the Na_2O is subsequently retained even after two ion exchange reactions with a 330-fold excess of ammonium ions. It is entirely likely that sodium ions are embedded in sites within the framework walls of the MCM-41 and therefore are not easily exchanged. Alkali metal ion impurities are known to labilize silica under hydrothermal conditions and thereby promote coarsening and densification.[40,41] An equivalent process most likely is responsible for the comparatively facile hydrothermal collapse of an MCM-41 mesostructure assembled from sodium silicate.

Further evidence for the role of framework sodium ions in compromising the hydrothermal stability of MCM-41 is provided by the sodium silicate doping experiments (cf., Figures 6 and 7). The addition of as little as 0.10 mol % Na_2O in the form of sodium silicate to a MCM-41 assembled from fumed silica reduces the surface area and framework pore volume to less than 50% and 25% of the respective initial values upon exposure to 20% steam at 800 °C for 5 h. The addition of 0.50 mol % Na_2O almost completely destroys the mesostructure under these conditions. Thus, even trace amounts of alkali metal ions must be considered in assessing the hydrothermal stabilities of silica mesostructures.

It should be emphasized that while the results of the present work point to the importance of embedded framework sodium ion impurities as the main cause of a greatly compromised hydrothermal stability of MCM-41, this conclusion applies only to mesostructures in which the local framework structures are comparable. In the absence of alkali metal impurities, the local framework structure is likely to play a very important role in determining the hydrothermal stability of a silicate mesostructure. Sodium-free mesostructures assembled from zeolite seeds, for instance, are much more stable under hydrothermal conditions than sodium-free mesostructures assembled from conventional framework precursors, even though the framework walls in both cases lack long-range atomic order.[15−18]

(37) Grimley, D. I.; Wright, A. C.; Sinclair, R. N. *J. Non-Cryst. Solids* **1990**, *119*, 49−64.
(38) Campbell, T.; Kalia, R. K.; Nakano, A.; Shimojo, F.; Tsuruta, K.; Vashishta, P.; Ogata, S. *Phys. Rev. Lett.* **1999**, *82*, 4018−4021.
(39) Pophal, C.; Fuess, H. *Microporous Mesoporous Mater.* **1999**, *33*, 241−247.
(40) Iler, R. K. *The Chemistry of Silica: Solubility, Polymerization, Colloid and Surface Properties and Biochemistry*; Wiley: New York, 1979.
(41) Brinker, C.; Scherer, G. *Sol−Gel Science: The Physics and Chemistry of Sol−Gel Processing*; Academic Press: New York, 1990.

Finally, we also note that the results of the present work are not at odds with the previously reported observation that the addition of appropriate amounts of sodium chloride in the assembly of MCM-41 from sodium silicate increases the hydrothermal stability of the end product.[25,42] Increasing the electrolyte concentration apparently increases the degree of framework cross-linking and alters the local structure of the silicate framework in the as-made mesostructure. The improvement in local framework structure, however, does not compensate for the deleterious effect of the residual framework sodium on the hydrothermal stability of the structure. That is, the local framework structure derived from fumed silica under sodium-free conditions provides substantially greater hydrothermal stability in comparison to a framework imbedded by sodium ions, even when the framework is assembled in the presence of excess sodium ion electrolyte.

Acknowledgment. We gratefully acknowledge the partial support of this research through NSF-CRG grant CHE-9903706. Use of the Advanced Photon Source was supported by the U.S. Department of Energy, Basic Energy Sciences, Office of Science, under Contract No. W-31-109-Eng-38. We are especially grateful for the expert help of the staff of MuCAT, in particular Doug Robinson, with the diffraction experiments. The Midwest Universities Collaborative Access Team (MUCAT) sector at the Advanced Photon Source (APS) is supported by the U.S. Department of Energy, Basic Energy Sciences, Office of Science, through the Ames Laboratory under Contract No. W-7405-Eng-82.

JA0118183

(42) Yu, J.; Shi, J.-L.; Chen, H.-R.; Yan, J.-N.; Yan, D.-S. *Microporous Mesoporous Mater.* **2001**, *46*, 153−162.